

Topological Fermi arcs

M.A. Silaev¹ and G.E. Volovik^{2,3}

¹ *Institute for Physics of Microstructures RAS, 603950 Nizhny Novgorod, Russia*

² *Low Temperature Laboratory, Aalto University, P.O. Box 15100, 00076 Aalto, Finland*

³ *L. D. Landau Institute for Theoretical Physics, 117940 Moscow, Russia*

(Dated: April 17, 2019)

We consider the Fermi arcs emerging on the domain wall in the Weyl superfluid ³He-A and at the interface between ³He-A and the fully gapped topological superfluid ³He-B.

PACS numbers:

I. INTRODUCTION

Chiral Weyl fermions represent the fermionic sector in the Standard Model of particle physics. The point nodes in the spectrum of chiral quarks and leptons are topologically protected, as well as their condensed matter counterparts, which are called Dirac or Weyl points (on topology of Weyl points in particle physics and condensed matter see e.g. Refs. 1–5).

The nodal topological systems with Weyl fermions demonstrate different types of the bulk-surface and the bulk-vortex correspondence. Due to bulk-vortex correspondence, the core of some vortices in the Weyl superfluid ³He-A contains the dispersionless branch of bound states with zero energy one-dimensional flat band, which was first discussed by Kopnin and Salomaa in 1991⁶. The end points of this flat band are determined by projections of the Weyl points to the direction of the vortex axis (see Refs. 7,8 for the topological origin of this flat band, and Refs. 9–12 for discussion of the topological flat bands in general). Due to bulk-surface correspondence, the surface of the system with Weyl points contains another exotic object – the Fermi arc – the 1D Fermi line in the 2D momentum space, which terminates on the projections of two Weyl points to the plane of the surface. The Fermi arc on the surface of ³He-A shown in Fig.1a has been considered in Ref. 13 and that on the surface of topological semi-metals with Weyl points – in Refs. 14–16. The flat band in the vortex core and the Fermi arc on the surface are the momentum-space analogs of the real-space Dirac string terminating on two magnetic monopoles⁹.

The similar Fermi arc appears at the interface between the ³He-A states with the opposite directions of the Weyl points. The bound states emerging at one of the representatives of such interface – the $\hat{\mathbf{l}}$ -soliton – has been calculated in Ref. 17. Here we consider the bound states emerging on the non-topological domain wall in ³He-A discussed in Ref. 18. The zero energy edge states on such domain wall in a thin film of ³He-A and the topological bulk-edge correspondence for this 2+1 system were considered in Ref. 19. The Fermi arc emerging in the 3+1 system forms a special configuration in momentum space, see Fig. 1b. We also consider the Fermi arc emerging at the interface between two topologically different quantum vacua: the ³He-A with Weyl points and the fully gapped

³He-B, which also has nontrivial topology in momentum space^{12,20–22} (AB interface).

II. SPECTRUM OF BOUND FERMIONIC STATES ON DOMAIN WALL IN SUPERFLUID ³HE-A

We calculate the spectrum of eigenstates of the Bogolyubov-de Gennes (BdG) Hamiltonian describing spin-triplet p -wave superfluids/superconductors

$$\hat{H} = [\varepsilon(p) - \mu]\hat{\tau}_3 + \hat{\tau}_1 \text{Re}\hat{\Delta} - \hat{\tau}_2 \text{Im}\hat{\Delta}, \quad (1)$$

where $\varepsilon(p) = (p_x^2 + p_y^2 + p_z^2)/2m$, $\hat{\Delta} = A_{\alpha i} \hat{\sigma}_\alpha p_i / p_F$, and $\hat{\tau}_i$ are Pauli matrices of Bogolyubov-Nambu spin, $\hat{\sigma}_\alpha$ are Pauli matrices of spin (in ³He it is nuclear spin). The order parameter is 3×3 matrix $A_{\alpha i}$ where the Greek and Latin indices correspond to the spin and orbital variables. Below we consider the fermionic modes localized on the different 1D order parameter defects, namely the domain wall of a ³He-A and the AB interface with order parameter inhomogeneity along the vector $\hat{\mathbf{n}} = \hat{\mathbf{x}}$ so that the momentum projections p_y and p_z are conserved.

A. Domain wall in ³He-A

We consider the configuration of one of the domain walls possible in ³He-A according to the symmetry classification – the one which is shown in Fig. 3a of Ref. 18. The orbital vector $\hat{\mathbf{l}}$ of the order parameter points down ($\hat{\mathbf{l}} \parallel -\hat{\mathbf{z}}$) as $x \rightarrow -\infty$ and points up ($\hat{\mathbf{l}} \parallel \hat{\mathbf{z}}$) as $x \rightarrow +\infty$. This domain wall configuration can be approximated by the following Ansatz:

$$A_{\alpha i}(x) = \Delta_0 \hat{d}_\alpha [\hat{x}_i + i f(x) \hat{y}_i], \quad (2)$$

where the unit vector $\hat{\mathbf{d}}$ represents the spin part of the order parameter, which is fixed if the spin-orbit interaction is neglected, and we put $\hat{\mathbf{d}} = \hat{\mathbf{x}}$. Then the gap function is given by

$$\hat{\Delta}_A = c_0 \hat{\sigma}_x [p_x + i f(x) p_y], \quad (3)$$

where $c_0 = \Delta_0 / p_F$ is the parameter which plays the role of the longitudinal speed of light in bulk ³He-A², $f(x)$ is

arbitrary function with asymptotics $f(\pm\infty) = \pm 1$. The topology of the bound states does not depend on the details of the function $f(x)$ if it is monotonic. Hereafter we shall choose the model form $f(x) = \tanh(x/r)$ where $r \sim \xi$ is width of the domain wall. The fermionic spectrum in this configuration was considered in Ref. 23 in quasiclassical approximation. Here we implement the analysis of the spectrum beyond the quasiclassics in order to study the zero energy states at the Fermi arcs supporting Majorana states.

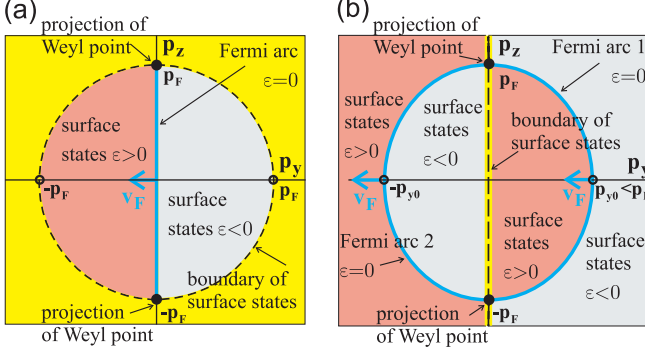


FIG. 1: (Color online) The zero energy branch of bound states spectrum $\varepsilon(p_y, p_z) = 0$ forms (a) the Fermi arc (solid blue line) on the boundary of ${}^3\text{He-A}$ according to Ref. 13; (b) two Fermi arcs on the domain wall in Eq.(2). Only single spin projection is considered. Thick arrows show directions of Fermi velocity at the Fermi arcs. In (a) the Fermi arc has topological charge $N = +1$, which satisfies the index theorem, which follows from the bulk-surface correspondence and the momentum space topology of Weyl points in bulk ${}^3\text{He-A}$. Fermi arc terminates on the projections of Weyl points to the surface of ${}^3\text{He-A}$. The spectrum of bound states terminates at the dashed line where the spectrum merges with the bulk spectrum. The region of continuous spectrum is shown by yellow shading. In (b) at $p_z = 0$ the Fermi velocity at the Fermi arcs is in the same direction, $\mathbf{v}_F = v_y \mathbf{y}$ where $v_y < 0$, which demonstrates that both Fermi arcs have the same topological charge $N = +1$, which together satisfy the index theorem $\tilde{N}_3(\text{left}) - \tilde{N}_3(\text{right}) = +2$, in agreement with momentum space topology of Weyl points in bulk ${}^3\text{He-A}$ on two sides of the domain wall in Fig. 3. Fermi arcs terminate on the projections of Weyl points to the interface. The spectrum of bound states has discontinuity at $p_y = 0$ where the spectrum merges with the bulk spectrum (the edge of continuum is shown by thick yellow line).

The continuous part of the spectrum $\varepsilon_c(\mathbf{p})$ of fermionic excitations is determined by the eigen states of Hamiltonian (1) at the bulk regions $|x| \gg r$

$$\varepsilon_c(\mathbf{p}) = \pm \sqrt{[\varepsilon(p) - \varepsilon_F]^2 + c_0^2(p_x^2 + p_y^2)}. \quad (4)$$

The states localized at the domain wall are characterized by single discrete quantum number which enumerates the energy branches and by the two continuous quantum numbers which are the projections of the quasiparticle momentum $p_{y,z}$ onto the domain wall plane. The

energy of localized states is confined within the region $|\varepsilon| < \min_{p_x} \varepsilon_c(\mathbf{p})$.

B. Semiclassical spectrum.

We begin the analysis of the spectrum of localized states from the semiclassical approximation. Provided the condition $p_x \xi \gg 1$ is valid we use the expression for the energy (4) substituting the local value of the order parameter. In this case we obtain

$$\varepsilon = \pm \sqrt{[p_x^2/(2m) - \mu_x]^2 + c_0^2[p_x^2 + f^2(x)p_y^2]}. \quad (5)$$

where $\mu_x = \varepsilon_F - (p_y^2 + p_z^2)/2m$. From Eq.(5) the function $p_x = p_x(x)$ can be found which describes semiclassical orbit in (p_x, x) phase space. In general the orbits can have two types of stationary points determined by the nature of quasiparticle reflection.

The normal reflection occurs at the points $x = x_{1,2}^n$ defined by $p_x(x_{1,2}^n) = 0$ or equivalently $c_0 p_y f(x_{1,2}^n) = \pm \sqrt{\varepsilon^2 - \varepsilon_{n2}^2}$ and exists at the energy interval $\varepsilon_{n2} < |\varepsilon| < \varepsilon_{n1}$ where $\varepsilon_{n1} = \sqrt{(c_0 p_y)^2 + \mu_x^2}$ and $\varepsilon_{n2} = \mu_x$. The Andreev reflection occurs at $x = x_{1,2}^a$ where $Im(p_x)$ becomes non-zero $c_0 p_y f(x_{1,2}^a) = \pm \sqrt{\varepsilon^2 - \varepsilon_{a2}^2}$ and exists if $\varepsilon_{a2} < |\varepsilon| < \varepsilon_{a1}$ where $\varepsilon_{a1} = c_0 \sqrt{p_y^2 + 2m\mu_x - (mc_0)^2}$ and $\varepsilon_{a2} = c_0 \sqrt{2m\mu_x - (mc_0)^2}$.

One can see that $\varepsilon_{n1} > \varepsilon_{a1}$ and $\varepsilon_{n2} > \varepsilon_{a2}$ therefore Eq.(5) determines two qualitatively different types of the enclosed quasiparticle orbits in (p_x, x) space. That is for the energies (i) $\varepsilon_{n1} > |\varepsilon| > \varepsilon_{a1}$ the orbits have only normal reflection points and for (ii) $\varepsilon_{n2} > |\varepsilon| > \varepsilon_{a2}$ only Andreev reflection points. The orbits of type (i) and (ii) are shown in the Fig.(2) by red dashed and green solid lines correspondingly. Provided (iii) $\varepsilon_{a1} > \varepsilon_{n2}$ there is also the third regime when the orbit has both normal and Andreev reflection points which is shown by the blue dash-dotted line in the Fig.(2). The energy spectrum is determined by the Bohr-Sommerfeld quantization $\oint p_x dx = 2\pi(n + \gamma)$ where $n = 1/2$ when the number of turning points is even²⁴.

From the above semiclassical consideration we obtain that the energy of localized states is not bounded as function of p_y and p_z . Indeed let us consider the case (i) and assume $\sqrt{\varepsilon^2 - \mu_x^2} \ll c_0 |p_y| \ll |\varepsilon|$. In this case the Taylor expansion can be implemented $f(x) = x/r$ in the Eq. (5) which yields then the harmonic oscillator spectrum

$$\varepsilon_n(p_y, p_z) = |\mu_x| + \omega(n + 1/2) \quad (6)$$

where $\omega = c_0(|p_y|/p_F r) \sqrt{2\varepsilon_F/|\mu_x|}$. One can see that the Eq.(6) yields $\varepsilon > |\mu_x|$.

Besides the energy branches determined by Bohr-Sommerfeld quantization with $n \geq 1$ there exists a so-called 'zero branch' of the spectrum which contains the zero modes $\varepsilon = 0$. This branch can not be obtained from the semiclassical approach therefore the different treatment is needed¹⁷.

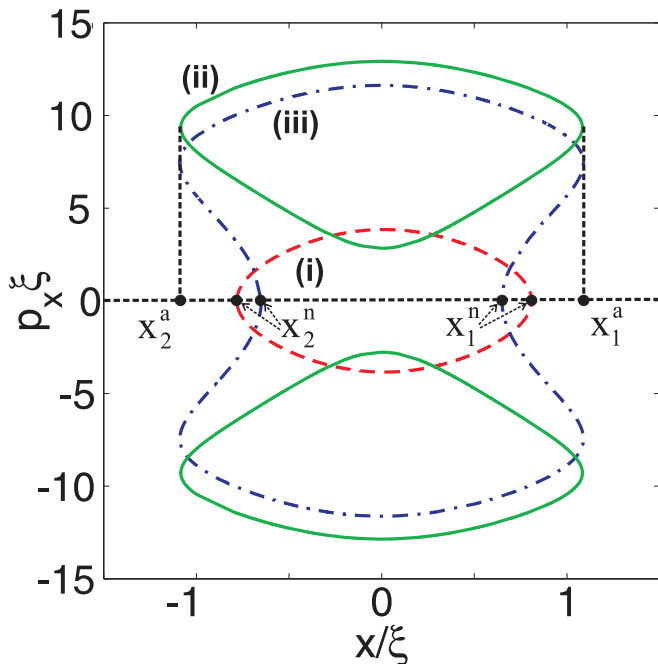


FIG. 2: (Color online) Closed orbits $p_x = p_x(x)$ determined by the semiclassical Eq.(5) at the domain wall for $p_z = 0$, $p_y = 0.5p_F$ and $c_0/v_F = 2.5 * 10^{-3}$. Shown by red dashed, green solid and blue dash-dotted curves are the regimes (i), (ii) and (iii) discussed in the text. The positions of Andreev $x_{a1,2}$ and normal $x_{n1,2}$ reflection points on the semiclassical orbits is indicated.

C. Quasiclassical approximation.

To find the zero branch analytically we consider the case when $(p_x/p_F)p_x\xi \gg 1$ which allows to use the quasiclassical approximation when p_x is a number and $[\varepsilon(p) - \varepsilon_F] = -iv_x\partial_x$ where the projection of the Fermi velocity on the x axis is $|v_x| = |p_x|/m = \sqrt{p_F^2 - p_z^2 - p_y^2}/m$. First let us transform the quasiparticle wave function $\psi = (u, v)^T$ to remove the spin dependence of the order parameter $\tilde{u} = \sigma_x u$, $\tilde{v} = v$. Then with the help of transformation

$$g_+ = v + u \quad (7)$$

$$g_- = v - u \quad (8)$$

the BdG equation acquires the form

$$\begin{pmatrix} h_+ & \varepsilon + c_0 p_x \\ \varepsilon - c_0 p_x & h_- \end{pmatrix} \begin{pmatrix} g_+ \\ g_- \end{pmatrix} = 0 \quad (9)$$

where $h_{\pm} = -iv_x\partial_x \pm ic_0 f(x)p_y$.

The system (9) can be transformed to the decoupled second-order equations

$$[\partial_x^2 + U_{0+} \cosh^{-2} x] g_+ = E g_+ \quad (10)$$

$$[\partial_x^2 + U_{0-} \cosh^{-2} x] g_- = E g_- \quad (11)$$

where $E = (r/\xi)^2 + \alpha^2 - (p_F\varepsilon/p_x\Delta_0)^2$, $U_{0+} = \alpha + \alpha^2$, $\alpha = rc_0p_y/v_x$ and $U_{0-}(p_y) = U_{0+}(-p_y)$. The Eq.(10) has eigenvalues

$$E_n = (1 + 2n - \sqrt{1 + 4U_{0+}})^2/4 = (n - \alpha)^2$$

where $n \geq 0$ is integer, which results in the quasiclassical spectral branches^{17,23}

$$\varepsilon_n = \pm \Delta_0 \frac{|p_x|}{p_F} \sqrt{2\alpha n - n^2 + (r/\xi)^2}. \quad (12)$$

Note that the energy branches (12) are twofold degenerate with respect to the sign change of p_x projection and by spin projection σ_x . The zero spectral branch is given by the Eq.(12) with $n = 0$

$$\varepsilon_0(p_y, p_z) = c_0 \text{sign}(p_y) |p_x|. \quad (13)$$

The zero branch spectrum (13) is shown in the Fig.(4a) by solid lines. At $p_y = 0$ the spectral branches are discontinuous.

The spectral branches with $n > 0$ given by Eq.(12) exist only in the limited range of parameters $|p_y|/(p_F\xi) \ll |p_x| < p_x^*$ where $p_x^* = |p_y|n/[n^2 - (r/\xi)^2]$ provided that $n > r/\xi$. At $p_x = p_x^*$ the branch merges continuum. Thus behaviour is demonstrated in Fig.(4b) where the energy branches (12) with $n = 0, 1$ are shown by dashed green lines as function of $\mu_x = \varepsilon_F - (p_y^2 + p_z^2)/2m$ for the parameters $r = \xi/2$ (width of the domain wall), $c_0/v_F = 2.5 * 10^{-2}$ and $p_y = 0.5p_F$.

D. Spectrum near the Fermi arcs.

As pointed out by Nakahara²³ all the quasiclassical branches (13) formally contain zero energy states at $p_x = 0$ but this expression is applicable if $|p_x|\xi \gg 1$. The behaviour of zero branch in the limit $p_x \rightarrow 0$ and arbitrary values of p_y and p_z can be found numerically by solving the eigenvalue problem for the Eq. (9). The resulting energy spectrum $\varepsilon = \varepsilon(\mu_x)$ is shown in the Fig.(4b) by solid, dash-double dotted and dash-dotted lines as the function of $\mu_x = \varepsilon_F - (p_y^2 + p_z^2)/2m$ for $n = 0, 1$. Remarkably the twofold degeneracy $p_x \rightarrow -p_x$ of the quasiclassical spectrum is broken at $0 < \mu_x \ll \varepsilon_F$ and at $\mu_x < 0$. Therefore each of the quasiclassical energy branches (13) found by Nakahara splits by two modes as $\mu_x \rightarrow +0$ and $p_x \rightarrow 0$. In accordance with general topological argument the only one zero branch remains shown in the Fig.(4b) by red solid line. Note that in contrast to the quasiclassical zero branch shown by green dashed line the exact zero branch ends at the Fermi level at finite value of $\mu_{x0} > 0$. This crossing point determines the position of the Fermi arc shown in the Fig.(1b) by blue solid lines. For example the Fermi arcs cross the line $p_z = 0$ at $p_y = \pm p_{y0}$ where $p_{y0} = \sqrt{2m(\mu - \mu_{x0})} < p_F$.

Near the Weyl point in the limit $p_y \rightarrow 0$ the behaviour of zero branch can be found analytically using

the approach¹⁹. We will treat the first term in the Hamiltonian (1) as perturbation. The rest of the terms form zero order Hamiltonian

$$\hat{H}_0 = \hat{\tau}_1 \hat{p}_x - \hat{\tau}_2 p_y f(x) \quad (14)$$

where $\hat{p}_x = -i\partial_x$. We assume the model form of the domain wall $f(x) = \tanh(x/r)$. The Hamiltonian (14) has zero energy eigen state with the wave function components $\psi_0 = (u_0, v_0)$

$$u_0 = 0 \quad (15)$$

$$v_0 = N^{-1/2} \cosh^{-\alpha}(x/r) \quad (16)$$

where $\alpha = rp_y$ and $N = \int_{-\infty}^{\infty} \cosh^{-2\alpha}(x/r) dx$. The perturbation of the zero energy level is given by

$$\varepsilon_0(p_x, p_y) = \frac{\bar{p}_x^2}{2m} - \mu_x \quad (17)$$

where $\bar{p}_x^2 = \langle \psi_0 | \hat{p}_x^2 | \psi_0 \rangle$. The Fermi arc is then given by

$$p_z^2 = p_F^2 - \bar{p}_x^2 - p_y^2 \quad (18)$$

In the limit $p_y \rightarrow 0$ we obtain $\bar{p}_x^2 = p_y^2$ so that the Fermi arc is given by $p_z^2 = p_F^2 - 2p_y^2$ and ends at $p_z = \pm p_F$ in accordance with general topological arguments.

E. Topology of Fermi arcs

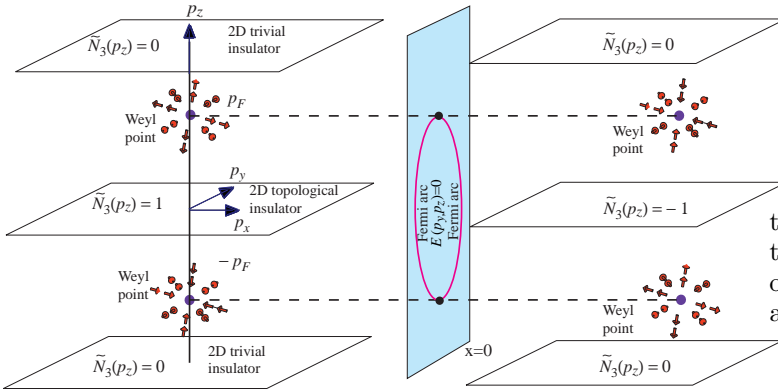


FIG. 3: Topology of the fermionic bound states on the domain wall in ³He-A. Momentum space topology of Weyl points in bulk ³He-A on two sides of the wall prescribes existence of the Fermi arcs in the spectrum of the fermionic states in the soliton or at the interface between the bulk states with different positions of Weyl points. In the considered case of the domain wall the Weyl points on two sides of the interface have the same positions in momentum space, but opposite topological invariants N_3 . This leads to two Fermi arcs terminating on the projections of the Weyl points to the plane of domain wall (Fig. 1b) according to the index theorem $\tilde{N}_3(\text{left}) - \tilde{N}_3(\text{right}) = 2$. This is distinct from the single Fermi arc on the surface of the ³He-A in Fig. 1a.

Let us compare the Fermi arcs on the domain wall in ³He-A with the Fermi arc on the surface of ³He-A. In both cases the Fermi arcs originate from the Weyl points in the bulk spectrum. But in case of the domain wall the Weyl points exist in the bulk liquids on both sides of the wall, as a result there are two Fermi arcs in Fig. 1b instead of a single Fermi arc in Fig. 1a. Topological origin of two Fermi arcs on the domain wall is demonstrated in Fig. 3. The Weyl points on two sides of the interface have the same positions in momentum space, but opposite topological invariants N_3 . The bulk spectrum in the plane with fixed p_z in momentum space has no nodes if $|p_z| \neq p_F$ and thus corresponds to the spectrum of 2D insulator. This insulator is topological for $|p_z| < p_F$, since it is described by nonzero topological invariant introduced in Refs. 25–28 for 2+1 systems:

$$\begin{aligned} \tilde{N}_3(p_z) &= \frac{1}{4\pi^2} \text{tr} \left[\int dp_x dp_y d\omega G \partial_{p_x} G^{-1} G \partial_{p_y} G^{-1} G \partial_\omega G^{-1} \right]. \end{aligned} \quad (19)$$

Here G is the Green's function matrix, which in our non-interacting models is $G = (i\omega - \hat{H})^{-1}$. One has $\tilde{N}_3(|p_z| < p_F) = +1$ on one side of the wall and $\tilde{N}_3(|p_z| < p_F) = -1$ on the other side. According to the index theorem^{2,19}, the difference between these two values determines the number of the zero modes at the interface between the 2+1 topological insulators for each $|p_z| < p_F$. As a result one has two Fermi arcs at the soliton wall.

III. BOUND STATES AT THE INTERFACE BETWEEN ³HE-A AND ³HE-B

Interestingly the problem of the fermionic spectrum of the states bound at the AB interface can be mapped on the case of domain wall of the A phase. Let us fix the order parameter on the B phase side of the interface, i.e. at $x = +\infty$, in the following form

$$A_{\alpha i}(x = +\infty) = \Delta_B (\hat{x}_\alpha \hat{x}_i + \hat{y}_\alpha \hat{y}_i + \hat{z}_\alpha \hat{z}_i). \quad (20)$$

The configuration of the A phase at $x \rightarrow -\infty$ can be different for different realizations of the domain wall (see e.g. Ref. 29). They are described by the relative orientations of the vectors $\hat{\mathbf{l}}$, $\hat{\mathbf{d}}$ and $\hat{\mathbf{n}}$ (the normal to the AB interface which in our case is $\hat{\mathbf{n}} = \hat{\mathbf{x}}$). First we shall consider the case $\hat{\mathbf{d}} = \hat{\mathbf{x}}$, $\hat{\mathbf{l}} = \hat{\mathbf{z}}$ which is claimed to have the lowest energy³⁰

$$A_{\alpha j}(x = -\infty) = \Delta_A \hat{x}_\alpha (\hat{x}_j - i\hat{y}_j). \quad (21)$$

We model the domain wall at the AB interface with $\Delta_A = \Delta_B = \Delta_0$ and the switching between bulk phases (21,20)

as follows

$$A_{xx} = \Delta_0 = \text{const} \quad (22)$$

$$A_{yy} = A_{zz} = \Delta_0 f_1(x) \quad (23)$$

$$A_{xy} = -i\Delta_0 f_2(x) \quad (24)$$

where $f_{1,2}(x)$ are the arbitrary monotonic functions with asymptotic $f_1(-\infty) = 0$, $f_1(+\infty) = 1$ and $f_2(-\infty) = 1$, $f_2(+\infty) = 0$.

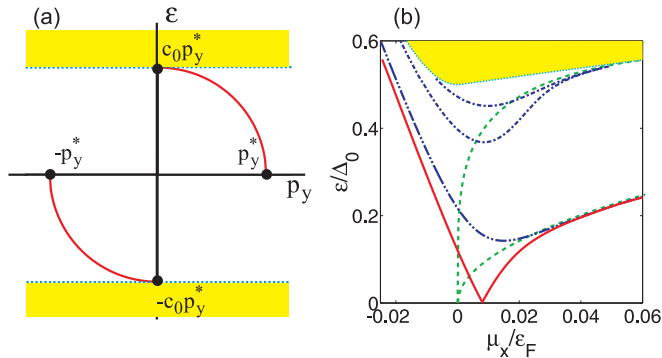


FIG. 4: (Color online) (a) Spectrum of the surface states at the domain wall of the A phase and at the AB interface $\varepsilon = \varepsilon(p_y)$ at fixed p_z given by Eq.(13). In case of the domain wall the spectrum is degenerate by spin σ_x while for the AB interface spin state is chosen such that $\sigma p_y > 0$. The discrete spectrum merges with continuum at $p_y = 0$ and the maximal energy of bound states is $\varepsilon_{max} = c_0 p_y^*$ where $p_y^* = \sqrt{p_F^2 - p_z^2}$. (b) Shown by solid red, blue dash-dotted and dash-double dotted lines are the spectral branches of localized states at the domain wall of A phase and AB interface for $\sigma = 1$ determined by the exact solution of BdG Eq.(1). The energy is plotted as function of $\mu_x = \mu - (p_y^2 + p_z^2)/2m$. The red solid line is the zero energy branch. The parameters are $r = \xi/2$ (width of the domain wall) and $c_0/v_F = 2.5 * 10^{-2}$, $p_y = 0.5p_F$. The branches of quasiclassical Eq.(12) found by Nakahara²³ are degenerate by $sign(p_x)$ and shown by green dashed lines for $n = 0, 1$. The degeneracy by $sign(p_x)$ is removed at the region $\mu_x \ll \varepsilon_F$ where each quasiclassical branch splits by two modes. In accordance with general topological argument the only one zero branch remains shown by the red solid line. The spectrum of delocalized states is shown by yellow shading and the edge of continuum by thin dotted line.

Let us transform the quasiparticle wave function components as follows $\tilde{u} = \sigma_x u$, $\tilde{v} = v$. Then we choose the spin basis $\chi_\sigma = (ip_z, p_\perp - \sigma p_y)$ where $\sigma = \pm 1$, $p_\perp = \sqrt{p_y^2 + p_z^2}$ so that the order parameter is diagonal in spin space $\hat{\Delta}(x) = c_0 [p_x + if_\sigma(x)]$ where

$$f_\sigma(x) = \sigma p_\perp f_1(x) - p_y f_2(x). \quad (25)$$

In order to obtain the bound states the function (25) has to satisfy the condition $f_\sigma(+\infty)f_\sigma(-\infty) < 0$ which yields $\sigma p_y > 0$. Employing the wave function transformation (7) we obtain the Eq.(9) with the exact eigenvalue

spectrum given by Eq.(13). In contrast to the case of the spectrum for the domain wall of the A phase considered above the spin degeneracy is removed since the proper spin state is determined by the condition of bound state existence $\sigma p_y > 0$. At $\mu_x \rightarrow +0$ and $\mu_x < 0$ the degeneracy of quasiclassical spectrum with respect to $p_x \rightarrow -p_x$ is removed analogously to domain wall of the A phase. The behavior of spectral branches for AB interface is the same to that shown in the Fig.(4b).

IV. DISCUSSION

We demonstrated that the Fermi arcs on the domain wall in the A-phase and at the interface between the A-phase and the B-phase of superfluid ³He-A obey the index theorem, which connects the topological properties of the bulk states on two sides of the walls with topology of the zero energy bound states. The domain wall in A-phase contains 4 Fermi arcs, if one takes into account spin degrees of freedom, while the AB interface contains 2 Fermi arcs, i.e. the same number as the surface of the A-phase. The reason for this difference is that the Fermi arc is determined by the Weyl points in the bulk states on two sides of the wall. The ³He-B, though being the topological superfluid, does not contain the Weyl point and thus does not contribute to the number of the Fermi arc.

The Majorana fermions living on the Fermi arc at the AB interface may give an additional contribution to the calculated friction force acting on the moving interface³¹ at very low temperatures. This is important for the development of the Kelvin-Helmholtz instability of the moving AB interface observed in Ref. 32 (see also Chapter 27 of Ref. 2). The latter instability has an analogue with the ergoregion instability of black holes discussed in Chapter 32 of Ref. 2.

We considered the simplest most symmetric realizations of the A-A and A-B interfaces. The problem for future investigations is whether the Fermi arc survives or not, if the symmetry of the interface is violated. For that the relative homotopy group formalism applied to Green's function³³ is probably required.

V. ACKNOWLEDGEMENTS

This work was supported, in part by the Academy of Finland (Centers of Excellence Programme 2012-2017), the EU 7th Framework Programme (FP7/2007-2013, Grant No. 228464 Microkelvin), by Russian Foundation for Basic Research Grant No. 11-02-00891-a, Presidential RSS Council (Grant No. MK-4211.2011.2), by Programs of RAS "Quantum Physics of Condensed Matter" and "Strongly correlated electrons in semiconductors, metals, superconductors and magnetic materials".

-
- ¹ C.D. Froggatt and H.B. Nielsen, *Origin of Symmetry*, World Scientific, Singapore, 1991.
- ² G.E. Volovik, *The Universe in a Helium Droplet*, Clarendon Press, Oxford (2003).
- ³ P. Hořava, Stability of Fermi surfaces and K -theory, Phys. Rev. Lett. **95**, 016405 (2005).
- ⁴ D.B. Kaplan and Sichun Sun, Spacetime as a topological insulator: Mechanism for the origin of the fermion generations, Phys. Rev. Lett. **108**, 181807 (2012).
- ⁵ M.A. Zubkov, Generalized unparticles, zeros of the Green function, and momentum space topology of the lattice model with overlap fermions, Phys. Rev. D **86**, 034505 (2012).
- ⁶ N.B. Kopnin and M.M. Salomaa, Mutual friction in superfluid ^3He : Effects of bound states in the vortex core, Phys. Rev. B **44**, 9667–9677 (1991).
- ⁷ G.E. Volovik, Flat band in the core of topological defects: bulk-vortex correspondence in topological superfluids with Fermi points, Pis'ma ZhETF **93**, 69–72 (2011); JETP Lett. **93**, 66 (2011).
- ⁸ T. Meng and L. Balents, Weyl superconductors Phys. Rev. B **86**, 054504 (2012); arXiv:1205.5202
- ⁹ T.T. Heikkilä, N.B. Kopnin and G.E. Volovik, Flat bands in topological media, Pis'ma ZhETF **94**, 252–258 (2011); JETP Lett. **94**, 233–239(2011); arXiv:1012.0905.
- ¹⁰ S. Ryu and Y. Hatsugai, Topological origin of zero-energy edge states in particle-hole symmetric systems, Phys. Rev. Lett. **89**, 077002 (2002).
- ¹¹ A.P. Schnyder and S. Ryu, Topological phases and flat surface bands in superconductors without inversion symmetry, arXiv:1011.1438; Phys. Rev. B **84**, 060504(R) (2011).
- ¹² G.E. Volovik, Topology of quantum vacuum, Chapter in proceedings of the Como Summer School on analogue gravity, arXiv:1111.4627.
- ¹³ Y. Tsutsumi, M. Ichioka, and K. Machida, Majorana surface states of superfluid ^3He A and B phases in a slab, Phys. Rev. B **83**, 094510 (2011).
- ¹⁴ A.A. Burkov and L. Balents, Weyl semimetal in a topological insulator multilayer, Phys. Rev. Lett. **107**, 127205 (2011); A.A. Burkov, M.D. Hook, L. Balents, Topological nodal semimetals, Phys. Rev. B **84**, 235126 (2011).
- ¹⁵ Xiangang Wan, A.M. Turner, A. Vishwanath and S.Y. Savrasov, Topological semimetal and Fermi-arc surface states in the electronic structure of pyrochlore iridates, Phys. Rev. B **83**, 205101 (2011).
- ¹⁶ P. Hosur, Friedel oscillations due to Fermi arcs in Weyl semimetals, arXiv:1208.0027.
- ¹⁷ T.L. Ho, J.R. Fulco, J.R. Schrieffer, F. Wilczek, Phys.Rev.Lett., **52**, 1524 (1984).
- ¹⁸ M.M. Salomaa, G.E. Volovik, Half-solitons in superfluid ^3He -A: Novel $\pi/2$ -Quanta of phase slippage, J. Low Temp. Phys, **74**, 319–346 (1989).
- ¹⁹ G.E. Volovik, Quantum Hall and chiral edge states in thin ^3He -A film, JETP Lett. **55**, 368–363 (1992).
- ²⁰ M.M. Salomaa and G.E. Volovik, Cosmiclike domain walls in superfluid ^3He -B: Instantons and diabolical points in (\mathbf{k}, \mathbf{r}) space, Phys. Rev. B **37**, 9298–9311 (1988).
- ²¹ A.P. Schnyder, S. Ryu, A. Furusaki and A.W.W. Ludwig, Classification of topological insulators and superconductors in three spatial dimensions, Phys. Rev. B **78**, 195125 (2008); A.P. Schnyder, S. Ryu, A. Furusaki and A.W.W. Ludwig, Classification of topological insulators and superconductors, AIP Conf. Proc. **1134**, 10 (2009); arXiv:0905.2029.
- ²² G.E. Volovik, Topological invariant for superfluid ^3He -B and quantum phase transitions, Pis'ma ZhETF **90**, 639–643 (2009); JETP Lett. **90**, 587–591 (2009); arXiv:0909.3084.
- ²³ M. Nakahara, Bound states on domain wall in superfluid ^3He -A film, J. Phys. C: Solid State Phys. **19** L195–L199 (1986)
- ²⁴ M.Ya. Azbel, Resonance and oscillatory effects in superconductors, ZhETF **59**, 295–313 (1970); JETP **32**, 159–168 (1971).
- ²⁵ H. So, Induced topological invariants by lattice fermions in odd dimensions, Prog. Theor. Phys. **74**, 585–593 (1985).
- ²⁶ K. Ishikawa and T. Matsuyama, Magnetic field induced multi component QED in three-dimensions and quantum Hall effect, Z. Phys. C **33**, 41–45 (1986).
- ²⁷ K. Ishikawa and T. Matsuyama, A microscopic theory of the quantum Hall effect, Nucl. Phys. B **280**, 523–548 (1987).
- ²⁸ G.E. Volovik and V.M. Yakovenko, Fractional charge, spin and statistics of solitons in superfluid ^3He film, J. Phys.: Condens. Matter **1**, 5263–5274 (1989).
- ²⁹ M.M. Salomaa, A phase transition of the moving superfluid ^3He A-B interface, J. Phys. C: Solid State Phys. **21** 4425 (1988).
- ³⁰ N. Schopohl, Spatial dependence of the order parameter of superfluid ^3He at the A-B phase boundary, Phys. Rev. Lett. **58**, 1664–1667 (1987).
- ³¹ N.B. Kopnin, Movement of the interface between the A and B phases in superfluid helium-3: linear theory, JETP **65**, 1187–1192 (1987).
- ³² R. Blaauwgeers, V. B. Eltsov, G. Eska, A.P. Finne, R.P. Haley, M. Krusius, J.J. Ruohio, L. Skrbek, and G. E. Volovik, Shear flow and Kelvin-Helmholtz instability in superfluids, Phys. Rev. Lett. **89**, 155301 (2002).
- ³³ J.I. Väyrynen and G.E. Volovik, Soft topological objects in topological media, Pis'ma ZhETF **93**, 378–382 (2011); JETP Lett. **93**, 344–348 (2011); arXiv:1101.1179.